A New Grid-Connected Asymmetrical Multilevel Converter for PV Application

Shayan Pourfarrokh, Jafar Adabi, and Firuz Zare, *Fellow, IEEE*

***Abstract*—In this article, an asymmetrical multilevel inverter (MLI) for employment in PV systems is introduced. Using a unidirectional isolated dc–dc converter at the input of the system, in addition to increasing the PV voltage level, prevents reverse power flow and can be used in high-power applications. This converter also isolates the PV source from the grid through a high-frequency transformer. The dc link of the system is connected to the grid by the proposed 25-level inverter, which significantly reduces the size of the grid inductor. Most switches of the proposed inverter operate at the fundamental and low frequencies, and the capacitors comprise the ability of self-balancing voltage. Also, the isolation between the sources of the proposed inverter can be done through a low-power isolated dc–dc converter. In addition to reducing the number of isolated sources, this converter always maintains the ratio between the inverter sources and stabilizes the quality of the output voltage. The injection of active power into the grid is managed by the proportional-resonant controller. Also, it is possible to exchange reactive power with the grid by the bidirectional proposed inverter. The proposed inverter is simulated in MATLAB software for verification and then implemented experimentally.**

***Index Terms*—Asymmetrical multilevel inverter (MLI), grid-connected converter, level-shifted modulation (LSM), proportional-resonant (PR) controller, PV application.**

I. Introduction

TODAY, grid-connected PV systems have been widely considered in various applications due to their numerous advantages [1], [2]. To eliminate the major disadvantages of common configurations, the multistring structure is used more. In this structure, the strings are connected to dc–dc converters that transfer the output voltage of PV strings to a common dc bus, and then a central inverter transfers the power to the grid [3].

In practice, the produced active power by PV arrays is inherently variable. Power quality issues caused by random characteristics of renewable energy and harmonics of inverters are fundamental problems when injecting power into the grid. In addition, the high-level penetration of grid-connected PV systems has caused concern for the facility [4], [5].

Generally, grid-connected PV systems are classified into two categories, isolated and nonisolated structures. Transformer-based grid-connected PV systems isolate the load from input changes and are more suitable for high-power systems [6]. In these systems, isolation is usually provided through a low-frequency transformer on the grid side which leads to many disadvantages such as high weight, low efficiency, and high cost. Also, the system limitations in the face of transient and impulse loads, as well as the increasing circulating current between the converters, are problems of nonisolated configuration [7]. High-frequency transformers are used to avoid problems of electrical isolation by line-frequency transformers [8]. For this reason, electrical isolation is preferred in the dc–dc stage.

At the same time, in transformerless grid-connected PV systems that use a conventional step-up circuit, the converter efficiency is reduced due to the boosting of the voltage level [9], [10]. In general, it is very difficult to choose between transformer-based and transformerless structures in grid-connected PV systems. In addition to mastering all existing structures, special features required for different applications should be considered [11].

In micro-grid applications, dc–ac converters are usually classified according to the number of stages, i.e., single-stage and double-stage systems. Grid-connected single-stage structures reduce the energy recovery capability of PV strings and are preferred for low-power applications [12]. Also, in double-stage systems, since the voltage level of PV panels is low, a converter with a high conversion ratio at the input and then an inverter is required for stand-alone ac load or grid-connected mode. Double-stage converters allow PV panels to operate by a centralized architecture over a wide range of voltage [13].

Meanwhile, in grid-connected PV systems, the dc–dc converter is an important stage for increasing the voltage level and electrical isolation between the PV modules and the inverter [14]. Isolated dc–dc converters are also used to compensate for deviations in PV panel voltage due to variations in radiation and temperature and to eliminate leakage currents in the PV module [15]. These converters can also implement the maximum power tracking algorithm for PV arrays. Fig. 1 shows the different types of PV inverters.

Since the cost per watt of the PV system is still high compared to other energy sources, current researches focus on both reducing production costs and increasing energy production in the system. In particular, the modern power converters as the

Manuscript received 23 January 2024; revised 25 April 2024; accepted 3 June 2024. Date of publication 13 June 2024; date of current version 16 July 2024. This work was supported by the Babol Noshirvani University of Technology under Grant BNUT/389051/1403. *(Corresponding author: Jafar Adabi.)*

Shayan Pourfarrokh and Jafar Adabi are with the Faculty of Electrical and Computer Engineering, Babol Noshirvani University of Technology, Babol 47148-71167, Iran (e-mail: sh.pourfarrokh@nit.ac.ir; j.adabi@nit.ac.ir).

Firuz Zare is with the School of Electrical Engineering and Robotics, Queensland University of Technology, Brisbane QLD 4000, Australia (e-mail: f.zare@qut.edu.au).

Color versions of one or more figures in this article are available at https://doi.org/10.1109/TPEL.2024.3414315.

Digital Object Identifier 10.1109/TPEL.2024.3414315

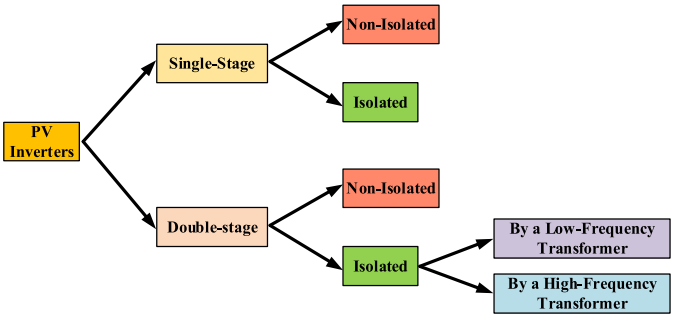

Fig. 1. Classification of PV inverters.

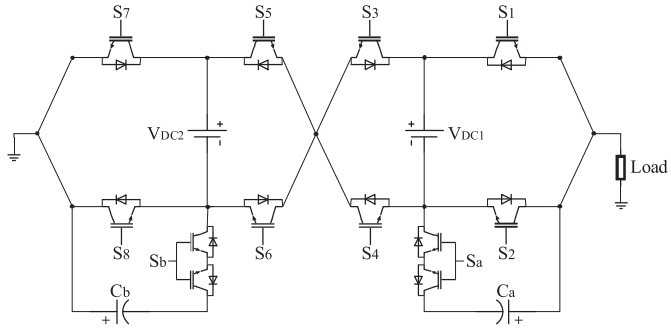

Fig. 2. Proposed inverter structure.

interface of PV modules to the grid have attracted the attention of researchers [16]. In general, the levelized cost of energy (LCOE) has been adopted to quantify and compare the cost of different PV systems. Accordingly, the inverter configuration, environmental conditions, reliability, and efficiency of the inverter, according to the scale of the PV array, affect the life of energy utilization and LCOE [17].

The optimal solution to reduce the LCOE index in a large-scale PV system is to use multilevel inverters (MLIs) instead of conventional two-level inverters [18]. This converter is also used to overcome power quality issues due to its harmonic properties and less electromagnetic interference noise. In addition, using an MLI can eliminate the need for a line-frequency transformer due to the reduction of the output total harmonic distortion (THD), and enable direct connection to the grid [19].

In the meantime, asymmetrical MLIs have become a popular structure among converters due to increasing the number of output levels while reducing switches [20]. However, some asymmetrical MLIs suffer from the inrush current problem due to the parallel charging of capacitors with sources [21]. In addition, using an H-bridge to produce negative output levels in some structures, leads to an increase in the total standing voltage (TSV) [22]. Also, the need for a large number of isolated sources [23], [24], [25] and using closed-loop control to balance the voltage capacitors are among the other problems of these converters. On the other hand, some asymmetrical structures do have not the ability of modularity because each bridge operates at a different voltage. Auxiliary bridges also restore power at some operating intervals [26]. At the same time, the modularity of PV systems has the advantages of increasing reliability, availability, simplicity of protection, and increasing the overall efficiency of the system in adverse conditions [27].

Meanwhile, structure [28] requires a special type of high-frequency transformer with multiple outputs to create isolated sources with different values for a CHB-based single-source asymmetrical MLI. Using this multiwinding transformer with a complex design for multilevel operation as well as a large number of passive devices limits the high-power applications for this structure. In [29] the high-frequency link (HFL) is used to generate isolated sources with different values through a variable source. This structure also suffers from a large number of passive devices and switches. In addition, the modularity of the structure is affected by the variable dc source and the high-frequency H-bridge, which causes increasing switching losses. Also, this structure does not create isolation between the PV and the grid. In multi-HFL converters, the number of devices increases significantly. In the structure [30] which is based on HFL, the need for additional floating capacitor control is visible, which results in lower voltage level, control complexity, and higher THD. Lack of isolation between PV and grid, the power limitation, and the modulation index of less than 0.85, limit the structure [31] for low-voltage applications. This structure also suffers from the problem of reverse power in auxiliary bridges. At the same time, the elimination of reverse power flow in dc–dc converters is essential [32]. For this purpose, some papers have suggested methods such as designing a specific angle of fire or adding surface jumping. The first method involves the complexity of system control and the second method increases the output THD.

To solve the mentioned problems in the previous structures, in this article, a grid-connected converter for PV applications is presented. The proposed inverter is given in Section II. In Section III, the general structure of the PV system is introduced. Simulation and experimental results of the proposed grid-connected inverter are given in Section IV. Finally, Section V concludes this article.

II. Proposed Asymmetrical MLI

In this section, the structure of the proposed asymmetrical 25-level inverter is introduced and the balancing of the capacitor voltage, the modulation method, and the modularity of the structure are explained.

Fig. 2 shows the topology of the proposed inverter, which belongs to asymmetrical MLIs with a combination of dc sources and capacitors. This type of structure is used to convert low-voltage dc sources to high-voltage ac output, especially in PV farms. To produce the maximum level of output voltage, asymmetrical sources with a quintuple sequence (V_{DC1} = 10E and V_{DC2} = 2E) have been used in the proposed structure. This topology includes two capacitors, and bidirectional switches that increase the output voltage levels from 9 to 25 compared to conventional structures.

In Table I, the switches, and capacitors status of the proposed inverter are specified at different output levels. Note that symbols ↑, ↓ and - are used to show the charging, discharging, and no change status of capacitors, respectively.

According to this table, the current path in different output levels is drawn in Fig. 3. In this way, blue paths for positive levels (blue box) and red paths for negative levels (red box) have been

TABLE I
SWITCHING TABLE OF THE PROPOSED INVERTER

States	Switches Status								Output Voltage	Level	Capacitors Status	
	S_1	S_2	S_a	S_3	S_5	S_7	S_8	S_b			C_a	C_b
1	1	0	0	0	1	0	1	0	$V_{DC1}+V_{DC2}$	+12E	-	-
2	1	0	0	0	1	0	0	1	$V_{DC1}+V_{DC2}-V_{Cb}$	+11E	-	↑
3	1	0	0	0	1	1	0	0	V_{DC1}	+10E	-	-
4	1	0	0	0	0	0	1	0				
5	1	0	0	0	0	0	0	1	$V_{DC1}-V_{Cb}$	+9E	-	↑
6	1	0	0	0	0	1	0	0	$V_{DC1}-V_{DC2}$	+8E	-	-
7	0	0	1	0	1	0	1	0	$V_{DC2}+V_{Ca}$	+7E	↓	-
8	0	0	1	0	1	0	0	1	$V_{DC2}+V_{Ca}-V_{Cb}$	+6E	↓	↑
9	0	0	1	0	1	1	0	0	V_{Ca}	+5E	↓	-
10	0	0	1	0	0	0	1	0				
11	0	0	1	0	0	0	0	1	$V_{Ca}-V_{Cb}$	+4E	↓	↑
12	0	0	1	0	0	1	0	0	$-V_{DC2}+V_{Ca}$	+3E	↓	-
13	0	1	0	0	1	0	1	0	V_{DC2}	+2E	-	-
14	0	1	0	0	1	0	0	1	$V_{DC2}-V_{Cb}$	+E	-	↑
15	0	1	0	0	1	1	0	0	0	0	-	-
16	1	0	0	1	0	0	1	0				
17	1	0	0	1	0	0	0	1	$-V_{Cb}$	-E	-	↓
18	1	0	0	1	0	1	0	0	$-V_{DC2}$	-2E	-	-
19	0	0	1	1	1	0	1	0	$-V_{DC1}+V_{DC2}+V_{Ca}$	-3E	↑	-
20	0	0	1	1	1	0	0	1	$-V_{DC1}+V_{DC2}+V_{Ca}-V_{Cb}$	-4E	↑	↓
21	0	0	1	1	1	1	0	0	$-V_{DC1}+V_{Ca}$	-5E	↑	-
22	0	0	1	1	0	0	1	0				
23	0	0	1	1	0	0	0	1	$-V_{DC1}+V_{Ca}-V_{Cb}$	-6E	↑	↓
24	0	0	1	1	0	1	0	0	$-V_{DC1}-V_{DC2}+V_{Ca}$	-7E	↑	-
25	0	1	0	1	1	0	1	0	$-V_{DC1}+V_{DC2}$	-8E	-	-
26	0	1	0	1	1	0	0	1	$-V_{DC1}+V_{DC2}-V_{Cb}$	-9E	-	↓
27	0	1	0	1	1	1	0	0	$-V_{DC1}$	-10E	-	-
28	0	1	0	1	0	0	1	0				
29	0	1	0	1	0	0	0	1	$-V_{DC1}-V_{Cb}$	-11E	-	↓
30	0	1	0	1	0	1	0	0	$-V_{DC1}-V_{DC2}$	-12E	-	-

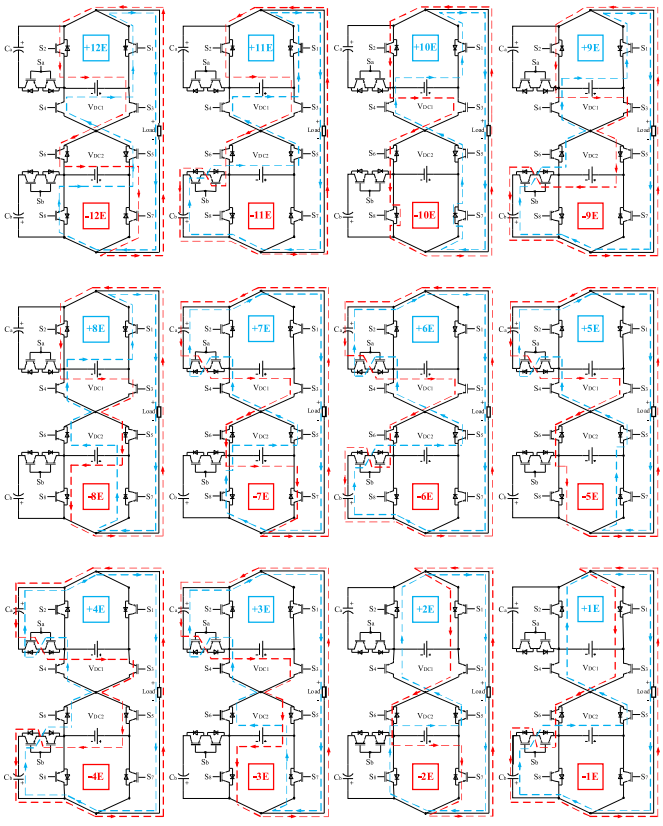

Fig. 3. Current path at different output levels of the proposed inverter.

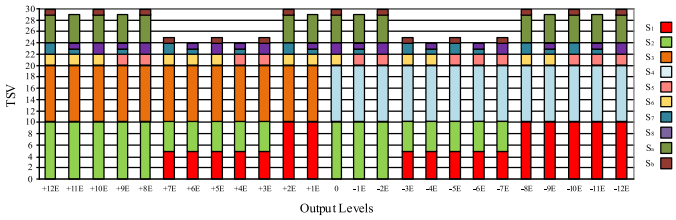

Fig. 4. TSV of the proposed inverter including blocking voltage by each switch at different output levels.

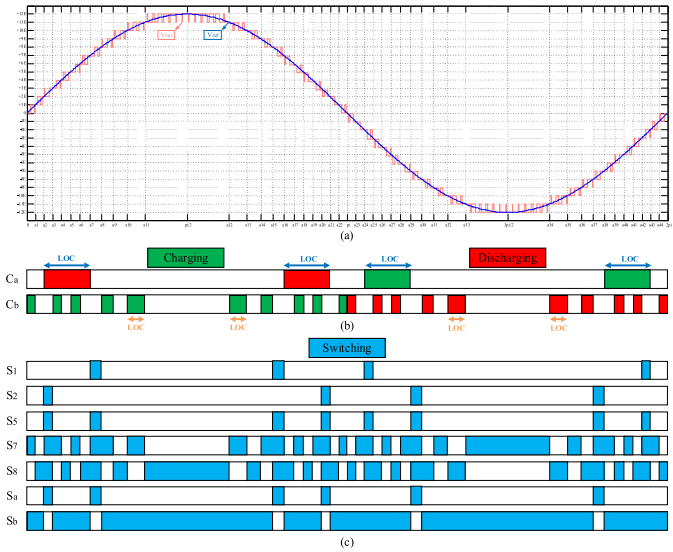

Fig. 5. (a) Output voltage levels. (b) Capacitors charging and discharging intervals. (c) Switching intervals of the proposed inverter.

merged in one figure for optimal display. Based on this figure, the capacitors are charged in series with the load in all cases. This prevents inrush currents during startup. Also, because of the same current path of S_3 and S_4 at all output levels, it is possible to remove the anti-parallel diode from these switches, and they can be single-quadrant switches. These switches can prevent the reverse flow of current when used in PV systems and are used for nonregenerative and stand-alone loads. Moreover, in Fig. 4, the TSV of the proposed inverter is demonstrated based on the switch status at different output levels. Also, in this figure, the contribution of each power switch in the tolerance of blocked voltage is displayed with different colors.

Fig. 5(a) shows the output voltage of the proposed 25-level inverter along with the reference voltage (blue waveform). The capacitors' voltages of the proposed topology are balanced inherently without using sensors and closed-loop controls and only through the modulation method. Thus, during an output period, the duration of charging and discharging capacitors at the same levels of the output voltage is equal [see Fig. 5(b)]. In this case, the capacitor voltage is fixed on half of the related source voltage.

The switching of the proposed structure is done based on the modified LSM method. According to this method, in the levels of the output waveform that have redundancies, a mode that has the least changes in the switches compared to the next level is

TABLE II
NUMBER OF OUTPUT LEVELS IN DIFFERENT MODES OF PROPOSED INVERTER

Ratio between Sources		N_L
Symmetrical		9
Binary		13
Trinary		17
Quadruple		21
Quintuple		25
Modular Structure		
1st Scenario	2 Modules	49
	n Modules	$24n+1$
2nd Scenario	2 Modules	625
	n Modules	$[4\sum_{n=0}^{2n-1}5^n]+1$

selected. For this reason, out of 36 possible switching modes in the proposed structure, 30 modes have been used according to Table I. This caused a significant reduction in switching losses in this structure. This type of power loss is one of the serious challenges in pulsewidth modulation (PWM) based methods.

Moreover, in the proposed inverter, the S_3 and S_4 are switched at the fundamental frequency by the modified LSM method. In this way, unlike the common methods where all the switches are operated in the carrier frequency, in the proposed structure, most of the switches are turned ON and OFF at the fundamental and low frequencies. In Fig. 5(c), the switching pulses are displayed during an output cycle, in which the switching regions have been marked in blue. Note that S_3 and S_5 are complementary to S_4 and S_6, respectively.

The proposed structure can also be used in high-power applications in a modular configuration. For this purpose, two methods have been used to connect the proposed inverter in cascade form. In the first scenario, the source voltage is the same in each module. In the second scenario, the source voltage of modules increases in quintuple sequence.

According to Table II, the number of output levels (N_L) based on the number of modules (n) is calculated in each method. Also, based on the application, the proposed structure can operate in other source sequences. The number of output levels in each sequence is mentioned in this table too.

In the current section, the capacitance of capacitors, power losses, and efficiency are also calculated. Moreover, a comparison is made between the proposed structure and other asymmetrical MLIs.

A. Calculation of Capacitances

Equation (1) is employed to calculate the capacitance of the proposed inverter capacitors

$$C_a \geq \frac{\Delta Q_1}{\Delta V_C\,(5E)} \quad \text{And} \quad C_b \geq \frac{\Delta Q_2}{\Delta V_C\,(E)}\,. \tag{1}$$

In the above equation, ΔV_C is the percentage of the capacitor voltage ripple, which is multiplied by the corresponding voltage level. Also, ΔQ is the flux deviation which is calculated based on the largest operation cycle parameter of the capacitors and the load current according to (2) and (3). In these equations, f_o and R_L are the output frequency and load resistance, respectively. Also, α is in radians and obtained using (4). Note that alpha values in Fig. 5(a) are calculated according to this equation.

$$\Delta Q_a = \frac{E}{2\pi f_o\,(R_L)}\,[3\,(\alpha_3-\alpha_2)+4\,(\alpha_4-\alpha_3)+5\,(\alpha_5-\alpha_4) + 6\,(\alpha_6-\alpha_5)+7\,(\alpha_7-\alpha_6)] \tag{2}$$

$$\Delta Q_b = \frac{E}{2\pi f_o\,(R_L)}\,[11\,(\alpha_{11}-\alpha_{10})] \tag{3}$$

$$\alpha_z = \sin^{-1}\left(\frac{z}{12}\right) \qquad \text{for} \quad 1 \leq z \leq 11. \tag{4}$$

By combining (1) to (3), the capacitance of each capacitor is calculated based on (5). Thus, in the proposed structure, the capacitor that has a higher capacitance withstands a lower voltage and vice versa

$$C_a \geq \frac{7\alpha_7-\alpha_6-\alpha_5-\alpha_4-\alpha_3-3\alpha_2}{10\pi f_o.\Delta V_C.R_L}\ \text{And}$$
$$C_b \geq \frac{11\,(\alpha_{11}-\alpha_{10})}{2\pi f_o.\Delta V_C.R_L}. \tag{5}$$

B. Power Loss Calculation

In general, the power losses of the proposed inverter include the conduction, switching, and capacitor ripple losses. Equation (6) is related to the calculation of the conduction loss, which is determined separately in each of the output levels (x) based on the equivalent circuit of the proposed structure. Note that the positive and negative levels have the same equivalent circuit

$$P_{Cx} = Vi + Ri^2\,. \tag{6}$$

In the above equation, V corresponds to V_{on} in the switch and V_d in the diode. Also, R refers to R_{on} in the switch, R_d in the diode, and R_c in the capacitor. As well, i is the load current.

In (7), the average conduction loss in each level is calculated according to its four times repetition in an output period

$$P_{Cx\text{avg}} = \frac{4\,(\alpha_x-\alpha_{x-1})}{2\pi}P_{Cx}. \tag{7}$$

The total conduction loss in all levels caused by 12 equivalent circuits of the proposed inverter is obtained as

$$P_{C\text{Total}} = \sum_{x=1}^{12} P_{Cx\text{avg}}. \tag{8}$$

Equation (9) is employed to calculate switching loss. In this regard, V_{CE} and I_C are the blocking voltage of the switch and the switch current, respectively. Also, f_{sw} is the switching frequency, as well as t_{on} and t_{off}, are the turning on and off times of the switch, respectively,

$$P_{\text{sw}j} = \frac{V_{\text{CE}}.I_C.f_{\text{sw}}}{6}\,(t_{\text{on}}+t_{\text{off}})\,. \tag{9}$$

According to the number of switches (j), the total power losses of the proposed inverter are determined according to

$$P_{\text{swTotal}} = \sum_{j=1}^{12} P_{\text{sw}j}. \tag{10}$$

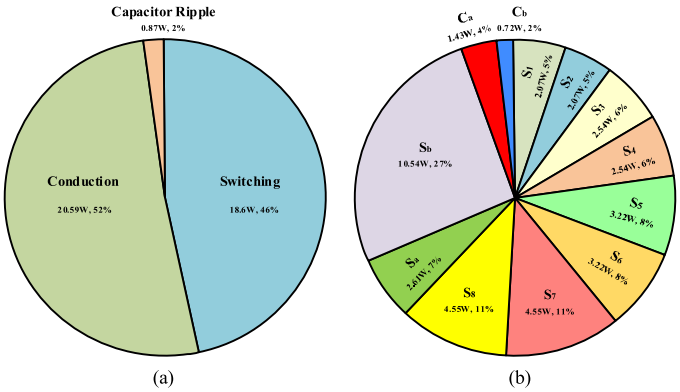

(a) (b)

Fig. 6. Power losses of the proposed inverter. (a) Contribution of power loss types. (b) Power loss of each device.

TABLE III
SPECIFICATIONS OF THE PROPOSED STRUCTURE

F_{cr}	m_a	N_L	RMS(v)	THD (%)	Efficiency (%)
5kHz	0.6	17	132	2.48	93.93
	0.7	19	154	1.68	95.72
	0.8	21	176	1.37	96.29
	0.9	23	198	1.09	96.54
4kHz	1	25	220	0.97	96.67
				1.15	
3kHz				1.39	

Calculation of the capacitor ripple loss is done through (11) in the largest operating time (LOT)

$$P_{Ry} = \frac{1}{2\mathrm{T}} C(\Delta V_C)^2 = \frac{1}{2T.C}\left[\int_{\mathrm{LOT}} i.dt\right]^2. \quad (11)$$

In the above equation, T refers to the output period. The sum of these losses is determined based on the number of capacitors (y) in the proposed inverter as

$$P_{R\mathrm{Total}} = \sum_{y=1}^{2} P_{Ry}. \quad (12)$$

Also, the total power loss (13) is calculated by (8), (10), and (12). Then, the efficiency of the proposed inverter is obtained based on the output power (P_{out}) according to (14)

$$P_{\mathrm{lossTotal}} = P_{C\mathrm{Total}} + P_{\mathrm{swTotal}} + P_{R\mathrm{Total}} \quad (13)$$

$$\eta = \frac{P_{\mathrm{OUT}}}{P_{\mathrm{OUT}} + P_{\mathrm{lossTotal}}} \times 100. \quad (14)$$

Based on the above equations, the power losses of the proposed inverter are accurately calculated when the output power has been considered 1 kW. Fig. 6(a) and (b) shows the contribution of power loss types and the power loss of each device in the proposed inverter, respectively.

Moreover, in Table III, the efficiency of the proposed inverter is obtained in different modulation indexes and switching frequencies. According to this table, by reducing the modulation index, the number of output levels is reduced, and as a result, the efficiency decreases and THD increases.

TABLE IV
COMPARISON OF THE PROPOSED STRUCTURE WITH OTHER ASYMMETRICAL 25LEVEL INVERTERS

Structure	N_{sw}	N_g	N_d	N_c	N_{dc}	$TSV_{P.U}$	Negative Level	Cost Function $\beta = 0.5$	Cost Function $\beta = 1.5$
[20]	12	12	14	2	2	5	Inherent	3.4	3.8
[21]	16	12	16	4	2	5	Inherent	4.04	4.44
[22]	16	14	14	2	2	6.8	With H-Bridge	3.95	4.5
[23]	12	12	16	-	4	5	Inherent	6.8	7.6
[24]	12	10	12	-	4	4.5	Inherent	5.8	6.52
[25]	12	12	12	-	4	4	Inherent	6.08	6.72
Proposed	**12**	**10**	**10**	**2**	**2**	**4.5**	**Inherent**	**2.9**	**3.26**

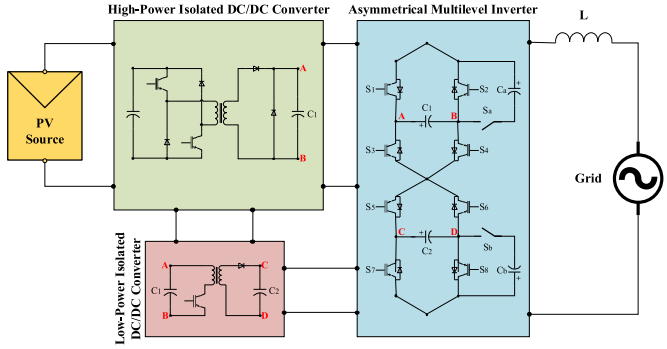

Fig. 7. Proposed PV system.

C. Comparative Study

In Table IV, the proposed inverter was compared with other recent asymmetrical 25-level inverters for a more accurate evaluation. Some parameters of this table include the number of switches (N_{sw}), gate drivers (N_g), diodes (N_d), capacitors (N_c), and sources (N_{dc}). Also, the ratio of TSV to the output voltage amplitude ($\mathrm{TSV}_{\mathrm{pu}}$), the generating method of negative output levels, and the cost function [which is calculated through (15)] are other parameters of Table IV

$$\mathrm{CF} = (N_{\mathrm{sw}} + N_g + N_d + N_c + \beta \times \mathrm{TSV}_{\mathrm{pu}}) \times \frac{N_{\mathrm{dc}}}{N_L}. \quad (15)$$

III. DESCRIPTION OF THE PV SYSTEM

Fig. 7 shows the overall structure of the PV system, which uses the proposed inverter to transfer the produced power by the PV cells to the grid.

In this system, to increase the voltage level of the PV cells and isolate the input from the grid, a high-power isolated dc–dc (HPIDC) converter can be used. The main isolated dc source (V_{C1}) of the proposed inverter is supplied directly by the output of the HPIDC converter. For this purpose, a dual-switch Forward converter is a suitable choice to operate at higher power. The switches of this converter use a common pulse. To prevent the saturation of the transformer, the duty cycle of this pulse should not be more than 50%. Due to its unidirectional structure, this converter also prevents the reverse power flow to PV sources, which is one of the main challenges in these systems. In addition, the high-frequency transformer in this converter isolates the PV source from the output, which is much smaller in volume

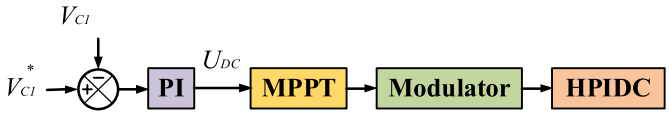

Fig. 8. Control diagram of the HPIDC converter.

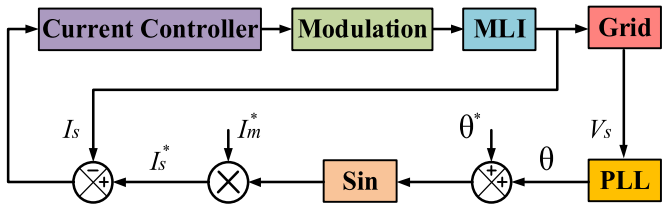

Fig. 9. Control algorithm of the proposed grid-connected inverter in the PV system.

and weight than line-frequency transformers, thus reducing the overall cost of the system.

On the other hand, using a flyback converter as a low-power isolated dc–dc (LPIDC) converter reduces the number of isolated sources required for the proposed MLI. This converter is supplied by the HPIDC converter and generates the second isolated dc source (V_{C2}) of the proposed inverter. The LPIDC converter is associated with high-frequency switches and only processes a small share of the output power. In this case, the high-frequency transformer of this converter will be small.

Besides, the switches related to the main source of the proposed inverter, which is responsible for processing most of the output power, are operated at the fundamental and low frequencies through the modified LSM method. This improves efficiency and makes the structure a suitable choice for high-power applications. Also, one of the most important features of the modulation method in grid-connected PV systems is the THD reduction of injected current to the grid. In the meantime, the LSM method can be a good option for these systems due to its simplicity and unique harmonic profits.

A. Control Method

Fig. 8 shows the control diagram of the HPIDC converter. According to this figure, V_{C1} is controlled to achieve MPPT by this converter and the controller can effectively manage the PV voltage along with V_{C1}, ensuring the MPPT algorithm. In this control method, first, V_{C1} is compared with its reference value ($V_{C1}{}^*$) and the error signal enters the PI controller. On the other hand, in grid-connected PV systems, the power of the PV module is proportional to the effective value of the output current, regardless of the system losses. This current is dependent on the output of the PI controller ($U_{\rm DC}$). Therefore, in this case, the MPPT algorithm can be implemented simply by using the signal $U_{\rm DC}$ [33]. At the same time, MPPT algorithms that use the output voltage and current of the PV module are costly and complicated.

Also, according to the proposed structure, one-fifth of V_{C1} must always be generated by the LPIDC converter. Therefore, to reduce the control complexity, an open-loop control method can be used for this converter. In this way, the duty cycle, and turn ratio of the isolated transformer in the mentioned converter are tuned to generate V_{C2} for the proposed MLI. If the main source of the proposed inverter does not have the nominal value, one-fifth of the main source is still transferred to the second source. This stabilizes the quality of the output waveform. In fact, due to using a single source in the structure, the proposed inverter sources are automatically balanced.

On the other hand, according to Fig. 9, the proposed grid-connected inverter of the PV system uses a closed-loop control algorithm to manage active power injection and reactive power exchange.

In the dual-loop current control method, first, the phase of the grid voltage (θ) is obtained by a phase-locked loop (PLL). Then the reference phase (θ^*), which is the phase difference between the grid voltage and current, can be added to the grid phase and determines the required power type. To inject the maximum active power into the grid, the reference phase should be considered zero. Also, to avoid reverse active power flow, the reference phase must be in the first and fourth quadrants. In addition, for injecting and consuming the reactive power by the inverter, the reference phase must be selected in the first and fourth quadrants, respectively.

In the next step, according to the amount of injected active power into the grid, the amplitude of the reference current ($I_m{}^*$) is determined and multiplied by the sine wave with the obtained phase of the previous step, and the reference current is created

$$I_s{}^* = I_m{}^* \sin(\theta + \theta^*). \tag{16}$$

According to (17) and (18), the grid current is determined by writing the KVL equation in the output loop

$$V_o - L_s\left(\frac{dI_s}{dt}\right) - V_s = 0 \tag{17}$$

$$I_s = \frac{1}{L_s}\int (V_o - V_s)\, dt\,. \tag{18}$$

In the above equations, V_o and L_s are the output voltage of the inverter and the grid inductor, respectively. The reference current is compared with the grid current in the inner loop based on (19) and the error signal (ε) will enter the current controller.

$$\varepsilon = I_s{}^* - I_s\,. \tag{19}$$

To eliminate the steady-state error in the grid current and also to make the system robust to input and grid changes, a proportional-resonant (PR) controller is employed [34]. According to (20), this controller improves the main harmonic of the grid current and reduces the low-order harmonics in this current and THD. In this equation, ω_c and ω_i are the angular cut-OFF, as well as the main and third-order frequencies, respectively. Also, K_p and K_{Ri} are the proportional and resonant coefficients of the main and third order harmonics in the PR controller, respectively,

$$V_o{}^* = \varepsilon\left[k_P + k_{R_1}\left(\frac{2\omega_c S}{S^2 + 2\omega_c S + {\omega_1}^2}\right)\right.$$

TABLE V
COMPARISON OF THE PROPOSED PV SYSTEM WITH OTHER SIMILAR STRUCTURES

Structure	DC/DC Stage					DC/AC Stage		System Characteristics					
	N_m	N_{sw}	N_d	N_c	N_t	N_{sw}	N_c	Asymmetric Source Ratio	M_{gain}	Isolation	N_L	Control Complexity	PV Application
[12]			-			12	2	1:1:3	1.67	No	9	Highest	No
[15]	3	1	5	6	1	12	0	1:3:9	M_{boost}(1.44)	No	27	Mid	Yes
[30]	2	8	4	6	2	12	1	1:2:4	M_{boost}(1.75)	Yes	15	Mid	No
[31]	2	4	0	4	1	12	2	1:3:9	1.23	No	27	High	Yes
Proposed	**1**	**3**	**5**	**2**	**2**	**12**	**2**	**1:5**	**M_{boost}**	**Yes**	**25**	**Low**	**Yes**

$$+ k_{R_3}\left(\frac{2\omega_c S}{S^2 + 2\omega_c S + {\omega_3}^2}\right)\Bigg] . \tag{20}$$

Finally, the reference voltage ($V_o{}^*$) is generated by the controller and the switching pulse is applied to the inverter switches through the LSM.

Moreover, in double-stage PV systems, due to changes in the output voltage of PV modules caused by temperature, irradiation, and MPPT, the dc link voltage of the inverter must be stabilized at the desired value. This duty in these systems is the responsibility of the inverter controller and is independent of the dc–dc converters. This prevents the dc–dc converter from operating in open-circuit conditions when the inverter starts up early. Therefore, in Fig. 9, $I_m{}^*$, as mentioned earlier, is determined based on $U_{\rm DC}$. Also, θ^* in this figure is determined based on the ratio of V_{C1} and $V_{C1}{}^*$. So if V_{C1} is more, then θ^* is positive and the reactive power is transferred to the grid. On the other hand, if V_{C1} is fewer, θ^* is negative and the reactive power is transferred from the grid to the dc-link capacitor. This compensates for dc link voltage changes during start-up and cloudy conditions, by using the bidirectional power flow capability of the proposed inverter.

B. Comparative Study

In this section, according to Table V, the introduced PV system has been compared to other related structures in different indicators including the number of devices, gain, isolation, the number of output voltage levels, the complexity of the control method, and usability in PV systems.

In this table, N_m, N_{sw}, N_d, N_c, N_t, and N_L represent the number of modules, switches, diodes, capacitors, transformers, and output voltage levels, respectively. In the PV system, the source sequence of the proposed inverter is quintuple, and unlike other structures, it only needs two isolated sources.

Also, in this table, $M_{\rm gain}$ shows the overall gain of the system. According to (21), this parameter is the ratio of the maximum output voltage and the input voltage value ($V_{\rm in}$). According to (22), $M_{\rm boost}$ is related to the turn ratio of the transformer and duty cycle of the switches in the HPIDC converter. Also, the gain of the proposed inverter will be equal to unity. In grid-connected PV systems, it is better to increase the voltage level in the first stage through a dc–dc converter. Because the boosting MLIs face a serious challenge due to voltage drop and high capacitance in the grid-connected mode.

$$M_{\rm gain} = \frac{\max\ (V_o)}{V_{\rm in}} \tag{21}$$

$$M_{\rm boost} = D_{fw}\frac{n_2}{n_1} . \tag{22}$$

TABLE VI
SIMULATION AND EXPERIMENTAL PARAMETERS OF THE PROPOSED INVERTER

Parameters		Value
V_{DC1}		260v
V_{DC2}		52v
C_a		470μF/150v
C_b		4700μF/30v
f_{cr}		5kHz
L_s		2.3mH
V_o		220v(RMS)
f_o		50Hz
P_o		1kW
Switches(IGBT)	(S_1~S_8)	2MBI75U4A-120
	(S_a&S_b)	K40H1203
Gate drivers		HCPL-316J
Voltage Sensor		MAU202
Current Sensor		LA55P
Digital Signal Processor (DSP)		TMS320f28335

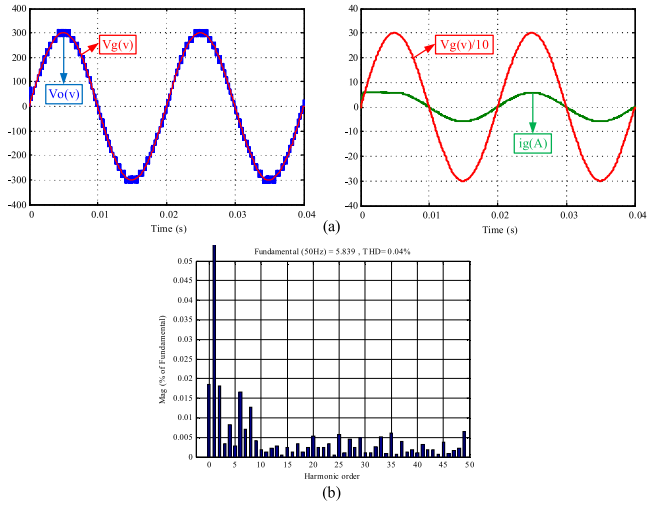

Fig. 10. (a) Output waveforms. (b) THD of output current at the simulated proposed grid-connected inverter.

In the mentioned system, the ratio of the number of levels to the number of devices is more than in similar structures. Also, this system isolates the sources from the grid, can be used in PV systems, and its control complexity is at the lowest level.

IV. SIMULATION AND EXPERIMENTAL RESULTS

In this section, the proposed inverter was first simulated in MATLAB-SIMULINK software and then implemented experimentally. The parameters' values of the proposed inverter are similar in both modes and are given in Table VI.

Fig. 10(a) shows the output voltage of the proposed inverter as well as the grid voltage and current during the injection of active power. Also, according to the FFT analysis in Fig. 10(b), the THD of injected current into the grid is much lower than the allowed limit in the IEEE 519 standard due to using the PR controller.

As shown in Fig. 11, finally the proposed system was implemented experimentally. In the closed-loop structure of the proposed system, the grid voltage and current are entered into the control algorithm through the sensor. Then, the switching

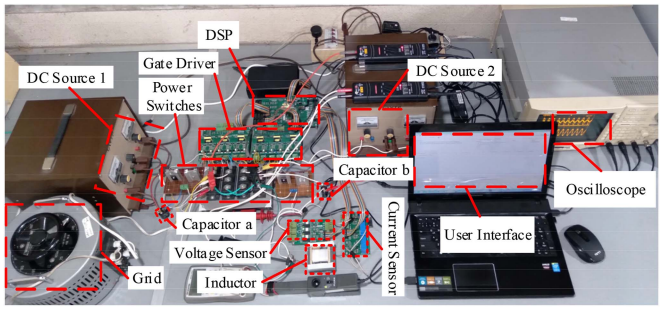

Fig. 11. Implemented proposed grid-connected inverter in the lab.

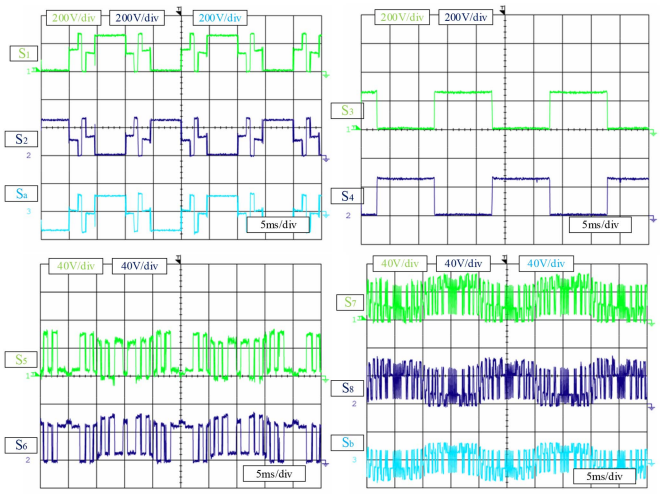

Fig. 12. Blocking voltage by power switches of the proposed inverter.

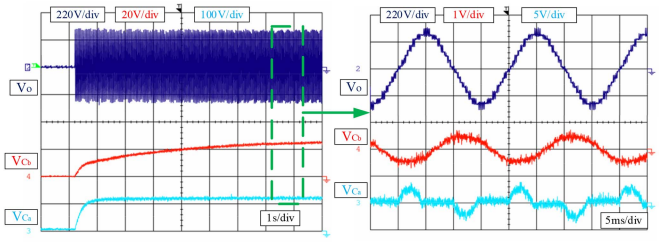

Fig. 13. Output voltage and capacitors voltage of the proposed inverter during the start-up.

pulse produced by the LSM method is applied to the switch driver and the power circuit.

Based on the output voltage of the proposed inverter which is related to the dc sources, the blocking voltage of the inverter switches is shown in Fig. 12. According to this figure, S_3 and S_5 are complementary with S_4 and S_6, respectively.

Fig. 13 demonstrates the output voltage of the proposed inverter and the capacitor voltage during startup. Based on this figure, without using closed-loop control, the capacitor voltage is stabilized through the self-balancing method on the desired level with the allowable ripple.

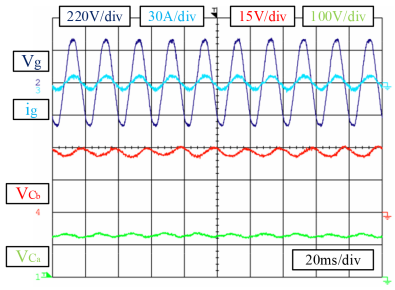

Fig. 14. Output waveforms and capacitors voltage of the proposed grid-connected inverter when injection of active power.

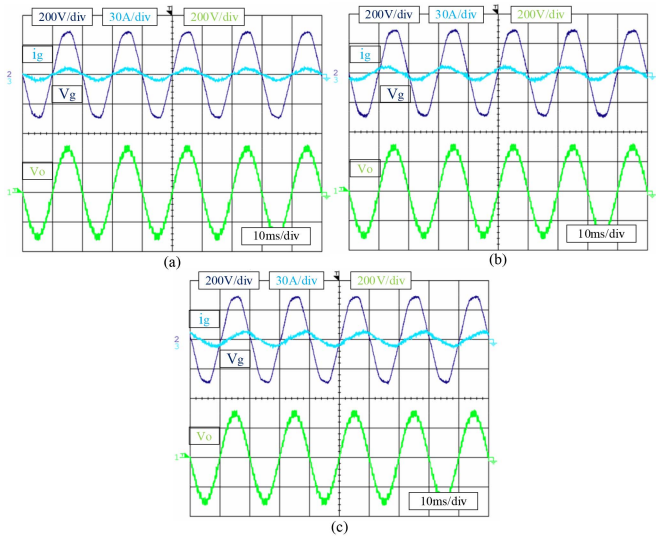

Fig. 15. Output waveforms of the proposed grid-connected inverter in the (a) in-phase, (b) lead, and (c) lag situation of the grid current.

Fig. 14 shows the capacitor voltage of the proposed inverter during active power injection. These capacitors are also fixed on 26 V and 130 V, respectively.

According to the phase sign of the reference current, active power injection into the grid or reactive power exchange is performed by the inverter, as shown in Fig. 15. In all cases, the 25-level output voltage is synchronous with the grid voltage through the PLL.

It is also possible to control the amount of power injected into the grid by changing the amplitude of the reference current in the control loop. In Fig. 16, the grid current is changed suddenly. The optimal performance of the system is retained in both modes.

In the last part of the implementation, two different scenarios for feeding the load by the grid-connected proposed inverter are considered. To estimate the dynamic performance of the system, step loads are supplied by the inverter in both scenarios. According to Figs. 17 and 18, in the first scenario, a linear load and in the second scenario, a non-linear load is placed in the output of the inverter, respectively. In these cases, the inverter provides the current of the step loads during the power injection into the grid and the output voltage of the inverter remains unchanged.

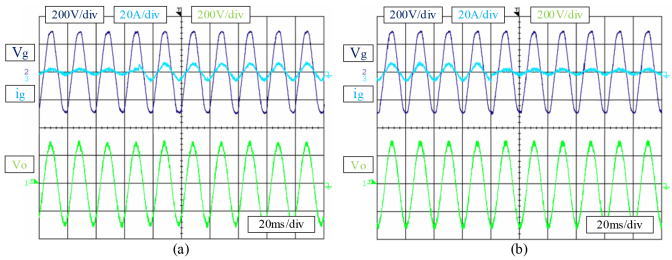

Fig. 16. Output waveforms of the proposed grid-connected inverter when (a) increasing grid current and (b) decreasing grid current.

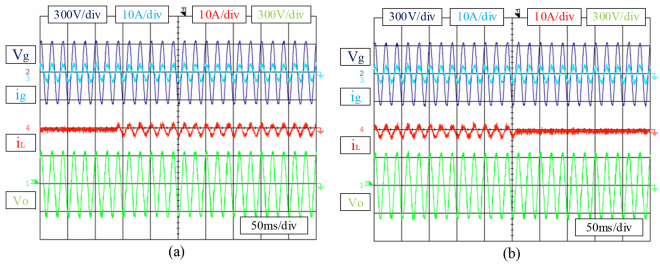

Fig. 17. Output waveforms of the proposed grid-connected inverter when (a) increasing linear load and (b) decreasing linear load.

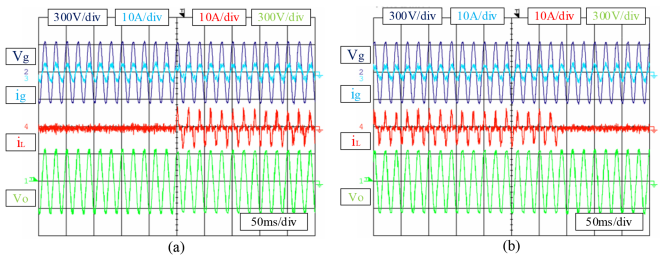

Fig. 18. Output waveforms of the proposed grid-connected inverter when (a) increasing nonlinear load and (b) decreasing nonlinear load.

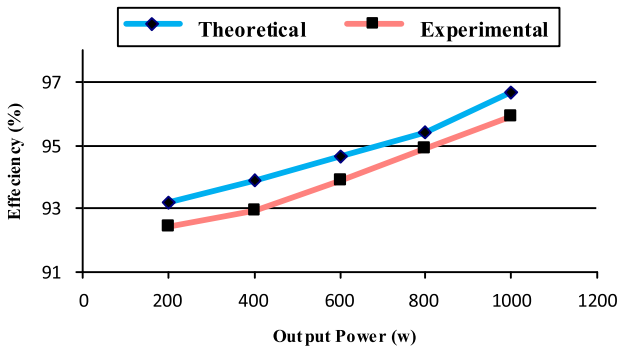

Fig. 19. Efficiency of the proposed inverter.

Finally, the efficiency curve of the proposed inverter in different output powers was obtained and plotted based on the theoretical calculation (see Section II-B), and experimental test as shown in Fig. 19.

V. Conclusion

In this article, a grid-connected asymmetrical MLI for PV applications was presented. The isolation between the input and the grid in the PV system could be done through the HPIDC converter. Thus, the size and weight of the transformer have been significantly reduced. This system could be implemented with a single source by the LPIDC converter. The proposed inverter including multiple advantages transmits power to the grid. The capacitors of the proposed inverter are charged in series with the load to avoid inrush current, and their voltage is balanced without the use of sensors or complex control algorithms. Also, the proposed inverter switches are operated at low frequencies to reduce switching loss and improve efficiency. The simple control algorithm could easily determine the type and amount of power exchange to the grid. Also, the proposed structure was compared in different parameters with the related converters presented in recent years. The obtained simulation and experimental results in different conditions demonstrated the optimal performance of the system.

References

[1] S. Kouro, J. I. Leon, D. Vinnikov, and L. G. Franquelo, "Grid-connected photovoltaic systems: An overview of recent research and emerging PV converter technology," *IEEE Ind. Electron. Mag.*, vol. 9, no. 1, pp. 47–61, Mar. 2015.

[2] K. Alluhaybi, I. Batarseh, and H. Hu, "Comprehensive review and comparison of single-phase grid-tied photovoltaic microinverters," *IEEE J. Emerg. Sel. Topics Power Electron.*, vol. 8, no. 2, pp. 1310–1329, Jun. 2020.

[3] E. Villanueva, P. Correa, J. Rodríguez, and M. Pacas, "Control of a single-phase cascaded H-bridge multilevel inverter for grid-connected photovoltaic systems," *IEEE Trans. Ind. Electron.*, vol. 56, no. 11, pp. 4399–4406, Nov. 2009.

[4] F. Blaabjerg, Y. Yang, K. A. Kim, and J. Rodriguez, "Power electronics technology for large-scale renewable energy generation," *Proc. IEEE*, vol. 111, no. 4, pp. 335–355, Apr. 2023.

[5] P. K. Chamarthi, A. Al-Durra, T. H. EL-Fouly, and K. Al Jaafari, "A novel three-phase transformerless cascaded multilevel inverter topology for grid-connected solar PV applications," *IEEE Trans. Ind. Appl.*, vol. 57, no. 3, pp. 2285–2297, May/Jun. 2021.

[6] J. Singh, R. Dahiya, and L. M. Saini, "Recent research on transformer based single DC source multilevel inverter: A review," *Renew. Sustain. Energy Rev.*, vol. 82, pp. 3207–3224, 2018.

[7] A. Mahfuz-Ur-Rahman, M. R. Islam, K. M. Muttaqi, and D. Sutanto, "Model predictive control for a new magnetic linked multilevel inverter to integrate solar photovoltaic systems with the power grids," *IEEE Trans. Ind. Appl.*, vol. 56, no. 6, pp. 7145–7155, Nov./Dec. 2020.

[8] S. Essakiappan, H. S. Krishnamoorthy, P. Enjeti, R. S. Balog, and S. Ahmed, "Multilevel medium-frequency link inverter for utility scale photovoltaic integration," *IEEE Trans. Power Electron.*, vol. 30, no. 7, pp. 3674–3684, Jul. 2015.

[9] E. A. D. Ibrahim, M. A. Gaafar, M. Orabi, A. Sheir, and M. Z. Youssef, "A novel dual-input high-gain transformerless multilevel single-Phase microinverter for PV systems," *IEEE Trans. Power Electron.*, vol. 35, no. 5, pp. 4703–4714, May 2020.

[10] J. Dadkhah, C. N. M. Ho, and K. K.-M. Siu, "Three-phase transformerless PV inverter with reconfigurable LCL filter and reactive power capability," *IEEE Trans. Power Electron.*, vol. 39, no. 7, pp. 8229–8241, Jul. 2024.

[11] M. B. Latran and A. Teke, "Investigation of multilevel multifunctional grid connected inverter topologies and control strategies used in photovoltaic systems," *Renew. Sustain. Energy Rev.*, vol. 42, pp. 361–376, 2015.

[12] S. Ziaeinejad and A. Mehrizi-Sani, "PWM a-CHB converter based on trinary multilevel converter: Topology, switching algorithm, and stability analysis," *IEEE Trans. Ind. Electron.*, vol. 66, no. 6, pp. 4166–4176, Jun. 2019.

[13] S. Dhara and V. Somasekhar, "An integrated semi-double stage-based multilevel inverter with voltage boosting scheme for photovoltaic systems," *IEEE J. Emerg. Sel. Topics Power Electron.*, vol. 8, no. 3, pp. 2326–2339, Sep. 2020.
[14] F. Amaral, T. Parreiras, G. Lobato, A. Machado, I. Pires, and B. Cardoso, "Operation of a grid-tied CMC based on a SiC forward SST under unbalanced PV power generation," *IEEE Trans. Ind. Appl.*, vol. 54, pp. 5493–5503, 2018.
[15] M. S. Manoharan, A. Ahmed, and J.-H. Park, "A PV power conditioning system using nonregenerative single-sourced trinary asymmetric multilevel inverter with hybrid control scheme and reduced leakage current," *IEEE Trans. Power Electron.*, vol. 32, no. 10, pp. 7602–7614, Oct. 2017.
[16] A. Mahfuz-Ur-Rahman, M. R. Islam, K. M. Muttaqi, and D. Sutanto, "A magnetic-linked multilevel active neutral point clamped converter with an advanced switching technique for grid integration of solar photovoltaic systems," *IEEE Trans. Ind. Appl.*, vol. 56, no. 2, pp. 1990–2000, Mar./Apr. 2020.
[17] M. Chen, Y. Yang, X. Liu, P. C. Loh, and F. Blaabjerg, "Single-source cascaded multilevel inverter with voltage-boost submodule and continuous input current for photovoltaic applications," *IEEE Trans. Power Electron.*, vol. 37, no. 1, pp. 955–970, Jan. 2022.
[18] T. Zhao and D. Chen, "A power adaptive control strategy for further extending the operation range of single-phase cascaded H-bridge multilevel PV inverter," *IEEE Trans. Ind. Electron.*, vol. 69, no. 2, pp. 1509–1520, Feb. 2022.
[19] S. Pourfarrokh, J. Adabi, and F. Zare, "A novel multilevel inverter with self-balancing capability of capacitors voltage; structure, modulation, and operation," *IEEE J. Emerg. Sel. Topics Power Electron.*, vol. 11, no. 2, pp. 1854–1864, Apr. 2023.
[20] E. Babaei and S. S. Gowgani, "Hybrid multilevel inverter using switched capacitor units," *IEEE Trans. Ind. Electron.*, vol. 61, no. 9, pp. 4614–4621, Sep. 2014.
[21] J. Ebrahimi, E. Babaei, and G. B. Gharehpetian, "A new multilevel converter topology with reduced number of power electronic components," *IEEE Trans. Ind. Electron.*, vol. 59, no. 2, pp. 655–667, Feb. 2012.
[22] S. Ramaiah, N. Lakshminarasamma, and M. K. Mishra, "Multisource switched capacitor based boost multilevel inverter for photovoltaic-based systems," *IEEE Trans. Power Electron.*, vol. 35, no. 3, pp. 2558–2570, Mar. 2020.
[23] R. Shalchi Alishah, D. Nazarpour, S. H. Hosseini, and M. Sabahi, "Novel topologies for symmetric, asymmetric, and cascade switched-diode multilevel converter with minimum number of power electronic components," *IEEE Trans. Ind. Electron.*, vol. 61, no. 10, pp. 5300–5310, Oct. 2014.
[24] R. Shalchi Alishah, D. Nazarpour, S. H. Hosseini, and M. Sabahi, "Reduction of power electronic elements in multilevel converters using a new cascade structure," *IEEE Trans. Ind. Electron.*, vol. 62, no. 1, pp. 256–269, Jan. 2015.
[25] R. S. Alishah, S. H. Hosseini, E. Babaei, and M. Sabahi, "A new general multilevel converter topology based on cascaded connection of submultilevel units with reduced switching components, DC sources, and blocked voltage by switches," *IEEE Trans. Ind. Electron.*, vol. 63, no. 11, pp. 7157–7164, Nov. 2016.
[26] M. Shahabadini and H. Iman-Eini, "Leakage current suppression in multilevel cascaded H-bridge based photovoltaic inverters," *IEEE Trans. Power Electron.*, vol. 36, no. 12, pp. 13754–13762, Dec. 2021.
[27] H. K. Jahan and M. Abapour, "Switched-capacitor-based multilevel inverter for grid-connected photovoltaic application," *IEEE Trans. Power Electron.*, vol. 36, no. 9, pp. 10317–10329, Sep. 2021.
[28] N. M. C. Mukundan, V. Kallaveetil, S. S. Kumar, and J. Pychadathil, "An improved H-bridge multilevel inverter-based multiobjective photovoltaic power conversion system," *IEEE Trans. Ind. Appl.*, vol. 57, no. 6, pp. 6339–6349, Nov./Dec. 2021.
[29] J. Pereda and J. Dixon, "High-frequency link: A solution for using only one DC source in asymmetric cascaded multilevel inverters," *IEEE Trans. Ind. Electron.*, vol. 58, no. 9, pp. 3884–3892, Sep. 2011.
[30] M. Lee, C.-S. Yeh, and J.-S. Lai, "A hybrid binary-cascaded multilevel inverter with simple floating-capacitor-voltage control," *IEEE Trans. Power Electron.*, vol. 36, no. 2, pp. 2218–2230, Feb. 2021.
[31] A. Ahmed, M. S. Manoharan, and J.-H. Park, "An efficient single-sourced asymmetrical cascaded multilevel inverter with reduced leakage current suitable for single-stage PV systems," *IEEE Trans. Energy Convers.*, vol. 34, no. 1, pp. 211–220, Mar. 2019.
[32] W. Liang, Y. Liu, and J. Peng, "A day and night operational Quasi-Z source multilevel grid-tied PV power system to achieve active and reactive power control," *IEEE Trans. Power Electron.*, vol. 36, no. 1, pp. 474–492, Jan. 2021.
[33] B. Yang, W. Li, Y. Zhao, and X. He, "Design and analysis of a grid-connected photovoltaic power system," *IEEE Trans. Power Electron.*, vol. 25, no. 4, pp. 992–1000, Apr. 2010.
[34] S. Pourfarrokh, A. Sheikholeslami, and A. AleAhmad, "Implementation of single-phase transformerless online uninterruptible power supply with multiple-resonant controller," *Iranian J. Sci. Technol., Trans. Elect. Eng.*, vol. 47, no. 3, pp. 1045–1058, 2023.

Shayan Pourfarrokh was born in Tehran, Iran, in 1993. He received the B.Sc., M.Sc., and Ph.D. degrees in electrical engineering with the focus on power electronics, in 2016, 2018, and 2022, respectively.

He is currently a research and development manager with the M.S.Pars Corporation, Tehran, Iran. His research interests include topology design, modulation techniques, multilevel inverters, uninterruptible power supplies, photovoltaic systems, and electric vehicles.

Jafar Adabi was born in 1981. He received the B.Eng. and M.Eng. degrees in power engineering from Mazandaran University, Babol, Iran, in 2004 and 2006, respectively, and the Ph.D. degree in power electronics from the School of Engineering Systems, Queensland University of Technology, Brisbane, QLD, Australia, in 2010.

He is currently a Professor with Babol Noshirvani University of Technology, Babol, Iran. His research interests include the optimal design and high-frequency modeling of power electronics and motor drive systems for electromagnetic interference analysis.

Firuz Zare (Fellow, IEEE) received the Ph.D. degree in power electronics from Queensland University of Technology, Brisbane, QLD, Australia, in 2002.

The Head of School of Electrical Engineering and Robotics at Queensland University of Technology in Australia. He has over 20 years of experience in academia, industry and international standardization committees, including eight years in two large R&D centres working on Grid Connected Inverters, Energy Conversion Systems and Power Quality Projects. He has been a very active member and leader in IEC, Danish and Australian standardization committees and has been a Task Force Leader (International Project Manager) of Active Infeed Converters to develop the first international standard IEC 61000-3-16 within the IEC standardization SC77A.

Dr. Zare was the recipient of several awards such as an Australian Future Fellowship, John Madsen Medal, Symposium Fellowship and early career excellence research award. He was also the recipient of a technology leadership program by the Danish Innovation Council, to attend one year leadership program delivered by Harvard Business School in Boston USA in 2015. He is a Senior Editor for IEEE ACCESS JOURNAL, a Guest Editor and an Associate Editor for IEEE JOURNAL OF EMERGING AND SELECTED TOPICS IN POWER ELECTRONICS and an Editorial board member of several international journals.